J Mater Sci (2015) 50:2849–2858
DOI 10.1007/s10853-015-8847-x

Enhanced antimicrobial activity with faceted silver nanostructures

Mauricio Rojas-Andrade · Adam T. Cho · Peiguang Hu · Shannon J. Lee · Christopher P. Deming · Samantha W. Sweeney · Chad Saltikov · Shaowei Chen

Received: 1 December 2014 / Accepted: 7 January 2015 / Published online: 24 January 2015

Abstract Faceted silver nanostructures including triangular nanoprisms, nanotetrahedra, and nanodecahedra were synthesized via a facile photochemical method at controlled wavelengths using spherical nanoparticles as the seeds. Scanning transmission electron microscopy studies showed that the resulting nanostructures were much larger in size (20–50 nm) than the spherical seed nanoparticles (under 5 nm), and X-ray diffraction as well as high-resolution transmission electron microscopy measurements confirmed that these nanostructures exhibited predominantly {111} faceted surfaces. Importantly, the silver nanostructures demonstrated markedly better antimicrobial activity than the spherical seed nanoparticles as evidenced by a lower minimum inhibitory concentration and more dramatic changes in both growth rate and lag phase at lower concentrations, which were attributed to the greater reactivity of the {111} faceted surfaces toward oxygen-rich bacterial surface moieties that allowed for more rapid localization to bacterial cells and increased interactions with structurally vital outer-membrane proteins. These results highlight the significance of surface morphologies of metal nanostructures in the manipulation of their antimicrobial activity.

Electronic supplementary material The online version of this article (doi:10.1007/s10853-015-8847-x) contains supplementary material, which is available to authorized users.

M. Rojas-Andrade · A. T. Cho · P. Hu · S. J. Lee · C. P. Deming · S. W. Sweeney · S. Chen (✉)
Department of Chemistry and Biochemistry, University of California Santa Cruz, California 95064, USA
e-mail: shaowei@ucsc.edu

C. Saltikov (✉)
Department of Microbiology and Environmental Toxicology, University of California Santa Cruz, California 95064, USA
e-mail: saltikov@metx.ucsc.edu

Introduction

The biocidal effects of silver have been known for thousands of years as there is evidence of ancient Greeks incorporating silver into wound dressings to stimulate healing and storing water in silver vessels for preservation [1]. The medical uses of silver have since expanded, as the first scientific publication on its effectiveness for treating newborn postpartum eye infections opened many scientists' curiosity and led to a surge of research into the applications of silver as a biocidal agent [2]. Silver has been found to be the most promising bactericidal agent in a plethora of scenarios, attributed to its exceptional activity at relatively low concentrations and limited toxicity toward eukaryotic cells [3]. Its effectiveness stems from its broad-spectrum effect on bacterial cells, as silver ions interact with multiple cellular targets affording the biggest advantage over target-specific, small-molecule antibiotics.

The mechanisms of silver toxicity have been thoroughly investigated by several groups, and there is general consensus on three primary mechanisms that lead to cell death: membrane lysis via peroxidation of structural lipids by reactive oxygen species (ROS), protein inactivation resulting from the binding and oxidation of thiol moieties on structurally relevant residues, and transcriptional arrest due to DNA condensation caused by the binding of silver ions to DNA molecules [4]. For instance, Kim et al. have shown evidence for ROS generation by silver ions through electron paramagnetic resonance (EPR) studies and membrane lysis of affected cells by transmission electron microscopy

(TEM), lending evidence for silver's role as an initiator of membrane peroxidation [5]. In the same study, the role of free radicals as active species was also supported as bacterial cultures having the antioxidant *N*-acetylcysteine added in addition to silver nanoparticles were found to have much higher survivability. Silver, as a soft acid, reacts preferentially with soft bases such as thiols which are essential components of protein tertiary structures. It has been shown that these soft–soft interactions are the underlying driving force behind silver's toxicity toward bacterial cells, as a study conducted by Xu et al. in 2012 comparing the toxicities of metal ions with varying softness found a trend in which softer metals such as silver, mercury, and cadmium demonstrated higher antimicrobial activity than harder metals such as zinc, nickel, and cobalt [6]. Several other groups have studied interactions of silver with thiol moieties of cysteine residues on proteins critical for cellular respiration, such as NADH dehydrogenase, which is responsible for causing cellular transcriptional arrest [7–10]. Additionally, silver has been found to react preferentially with N^7 of the GC and AT base pairs of DNA and not the phosphate groups of the DNA backbone as previously thought, resulting in helix condensation and transcriptional arrest [11]. Due to the multitude of mechanisms by which silver elicits its antimicrobial activity, it has become the most promising candidate for antimicrobial applications such as surface coatings, medical wound dressings, and water filtration.

With the advent of nanotechnology, highly effective silver nanostructures have now been developed which have a markedly enhanced activity when compared to silver salts [5, 12–15]. Recent advancements have been made in delivery mechanisms for biocidal silver, with hydrogels, polymers, and porous structures such as zeolites being utilized for both structural support and release of silver ions [16–18]. This improved activity is largely attributed to silver nanostructures having an exceptionally large surface-area-to-volume ratio with smaller particles having a larger degree of exposed surface area. This enhanced active surface area affords a greater level of contact with bacterial cell walls and allows for increased rates of silver ion dissolution thereby resulting in higher bactericidal activity [19]. Pal et al. recently found evidence that bactericidal activity is also shape-dependent, with triangular silver nanoprisms having predominantly {111} facets demonstrating superior activity when compared to spherical and cubical nanoparticles of similar size [20]. This study indicates that the activity is highly dependent on surface structure and suggests that the silver {111} facet is most favorable for antimicrobial applications due to its high atom density. This surface structure not only increases the likelihood of silver atoms binding to bacterial cell membrane and cell wall constituents but also enhances dissolution rate of silver atoms from the nanoparticle surface via oxidation by molecular oxygen and hydroxide molecules as evidenced by cyclic voltammetry studies comparing the dissolution between different silver facets [21]. Given the evidence, nanostructures with predominantly {111} faceted surfaces warrant further investigation to shed light on the nature of their enhanced antimicrobial activity. This is the primary motivation of the present study.

Photochemical synthesis of silver nanoprisms has gained much attention since Jin et al. first reported a simple light-induced ripening of silver nanospheres into nanoprisms [22]. This process was found to produce triangular, hexagonal, and circular nanoplates which were nearly flat (<10 nm thick) in high yield. The growth of these anisotropic nanostructures is the result of excitation of nanoparticle surface plasmon resonance (SPR) causing redox processes to occur preferentially at surfaces with more intense induced electromagnetic fields. Specifically, when the in-plane dipole resonance is excited, "hot" electrons and "hot" holes are generated and concentrated at surfaces on the nanoparticle in the same plane as the dipole excitation. At these surfaces, "hot" holes oxidize surface-bound citrate molecules into 1,3-acetonedicarboxylate and carbon dioxide though the photo-Kolbe mechanism, where the hydroxyl group of sodium citrate donates an electron pair to the central carbon atom forming a carbon–oxygen double bond which subsequently causes the central carbon to undergo heterolytic cleavage with the rest of the citrate molecule thereby releasing carbon dioxide [23]. NMR studies have previously shown supporting evidence of emerging 1,3-acetonedicarboxylate, with a corresponding peak at $\delta = 3.49$ ppm, upon photoexcitation of the silver nanospheres into triangular nanoprisms [24]. Localization of hot holes onto surface-bound citrate molecules initiates these irreversible decarboxylation reactions which transfer electrons to the silver nanoparticle causing in-plane surfaces to charge cathodically. This subsequently reduces Ag^+ ions in solution to Ag^0 resulting in selective in-plane growth [23–25]. Triangular nanoprisms are found to have a maximum-induced electromagnetic field localized at the tips from electron energy loss spectroscopy (EELS) when their in-plane SPR is excited. This allows for these photo-induced redox cycles to occur most rapidly on these surfaces, which explains why these structures dominate the final particle population after prolonged irradiation. This has indeed been observed experimentally [26]. Such a plasmon-mediated growth method provides a unique control of the structural morphology through synthetic parameters such as pH, silver ion concentration, citrate concentration, and most interestingly, excitation wavelength [27–29]. Triangular nanoprisms with varying edge-length have indeed been synthesized using the same synthetic conditions by merely varying the photoirradiation wavelength to excite the in-plane surface plasmon. Recently, light-emitting diodes (LEDs) have also been utilized as cost-effective radiation

sources and found to produce triangular nanoprisms similar in morphology and at equivalent yields [25, 30]. These resulting nanoplate structures have predominantly {111} faceted surfaces, providing a facile, energy-efficient method for the synthesis of anisotropic silver nanostructures that can be utilized to shed light on the structural root of silver nanoparticle antimicrobial activity.

In this study, a facile photochemical synthesis route is used for the preparation of anisotropic silver nanostructures by utilizing LEDs as the radiation source and only sodium citrate as the stabilizing agent. The resulting nanostructures were found to be markedly larger than the silver seed nanoparticles and comprised predominantly {111} surfaces as evidenced by HRTEM and XRD measurements. The antimicrobial efficacy of these faceted nanostructures was quantified and compared to that of the silver seed nanoparticles within the context of MIC, growth rates, and lag-phase duration over a dilution series. The results indicate that the antimicrobial activity is sensitively dependent on the nanoparticle surface morphologies.

Experimental section

Materials

Silver nitrate (99.9 %, STREM Chemicals), sodium citrate dihydrate (Fisher), sodium borohydride powder (98+ %, ACROS), Miller Luria broth (Fisher), and 4-(2-hydroxyethyl)-1-piperazineethanesulfonic acid (HEPES, 1 M, GIBCO) were used as received. All solvents were obtained from typical commercial sources and used without further treatment. Water was supplied by a Barnstead Nanopure water system (18.3 MΩ cm).

Photochemical synthesis of faceted silver nanostructures

To prepare faceted silver nanostructures, silver seed nanoparticles were first synthesized through reduction of silver nitrate (0.1 mM) with sodium borohydride (0.5 mM) in the presence of sodium citrate (0.6 mM). In brief, a 250 mL three-neck flask was filled with 96.5 mL of nanopure water, and to this, 0.5 mL of 20 mM silver nitrate and 2 mL of 30 mM sodium citrate were added. The flask was bubbled with nitrogen for 30 min in an ice bath; then 1 mL of a freshly prepared, 50 mM ice-cold sodium borohydride solution was added rapidly under vigorous stirring. The solution initially turned pale yellow, then gradually into brighter yellow after about 5 min of stirring indicating the formation of small silver nanoparticles. This solution was stirred for 10 min to allow for complete reduction, and then the flask was removed from the ice bath and placed between two 40 W blue LEDs (Hongke Lighting $\lambda_{em} = 455$–475 nm) for up to 24 h, leading to the production of silver nanostructures of varied shapes.

Characterizations

HRTEM images were acquired with a Phillips CM300 at 300 kV, and STEM images were taken by a FEI Quanta 3D FEG dual beam SEM/FIB. About 300 individual nanostructures were counted in HRTEM and STEM images to determine particle size and shape distributions. XRD patterns were collected with a Rigaku SmartLab PXRD within the range of 20° to 80° (2θ) at a rate of 1°/min and a 0.02° step size under CuKα radiation ($\lambda = 1.5418$ Å). Solutions of the samples were first mixed with acetonitrile at a 1:1 ratio and lyophilized for 48 h. The resulting solid was then placed on a glass microscope slide for characterization and analyzed using PDXL-2 software. UV–vis spectra were acquired by an Agilent Cary-60 UV–vis spectrometer, and bacterial optical density was measured in a Molecular Devices VERSAmax microplate reader.

Bacterial growth kinetics

Escherichia coli (ATCC# 25922) was first grown by spreading frozen liquid culture (20 % glycerol, −72 °C) on Luria broth (LB) agar and incubating at 37 °C overnight. From this plate, a single colony was selected and used to inoculate 3 mL of liquid LB and allowed to shake at 37 °C for 18 h. The resulting overnight liquid culture was centrifuged at 5000 rpm for 5 min and re-suspended in a sterile aqueous 20 mM HEPES solution. The re-suspension was diluted with fresh HEPES solution to an optical density of 0.10 at 600 nm and used for inoculation. A 96-well plate was used to contain all of the growth solutions with each wellbeing filled to a final volume of 200 μL with 80 μL of sterile LB, 20 μL of the inoculation solution, and varying volumes (100, 90, 80, 70, 60, 50, and 40 μL) of each antimicrobial agent and enough water to bring the final volume to 200 μL. Immediately upon inoculation, the 96-well plate was placed in the plate reader where the optical density at 600 nm for each well was measured every minute with 10 s mixing periods between reads over the 18 h incubation period at 37 °C.

Results and discussion

Photochemical synthesis of faceted silver nanostructures

Silver seed nanoparticles were first prepared by chemical reduction of silver nitrate with sodium borohydride in the presence of sodium citrate in water. Figure 1a depicts a

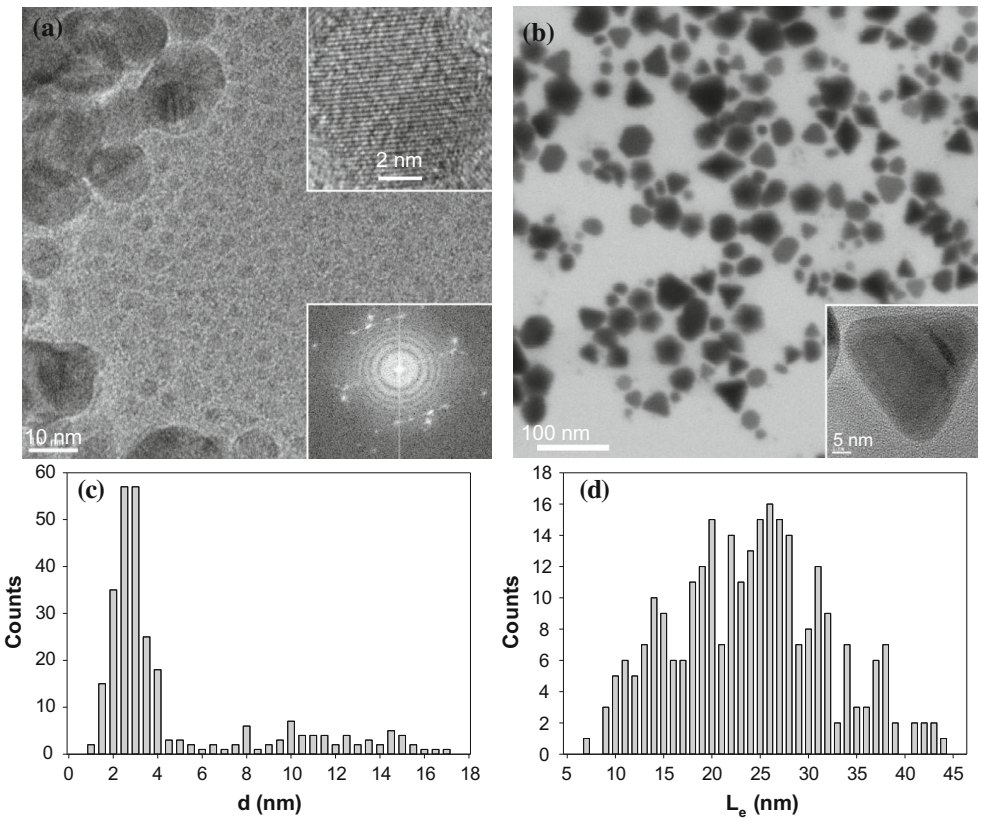

Fig. 1 Representative TEM images of **a** silver seed nanoparticles and **b** nanostructures prepared by photoirradiation for 24 h. *Scale bar* in **a** 10 and 200 nm in **b**. Top *inset* to pane **a** is a representative HETEM image that highlights the silver lattice fringes (*Scale bar* 2 nm) and the *bottom inset* is a diffraction pattern acquired from selected-area electron diffraction. *Inset* to panel **b** is a representative HRTEM image of a silver nanoprism. *Scale bar* 5 nm. Histograms of **c** particle diameter for silver seed nanoparticles and **d** edge-length for photo irradiated nanoparticles

representative TEM micrograph of the resulting nanoparticles. One can see that the seed nanoparticles are mostly spherical in shape, and statistical analysis based on about 300 nanoparticles showed a nearly unimodal distribution of the particle size with approximately 80 % of the particles having a diameter less than 5 nm, and the average diameter was estimated to be 4.76 ± 3.88 nm, as manifested in the core size histogram in panel (C).

In addition, well-defined crystalline lattice fringes can be seen in high-magnification TEM studies, as manifested in the top inset to panel (A) where the lattice spacing was estimated to be 0.231 nm, closely matching the value for *fcc* Ag(111) planes [31]. Consistent results were obtained in selected-area electron diffraction (SAED) that is depicted in the lower inset, where the circles are consistent with *fcc* Ag(111). Interestingly, three dotted lines can also be seen, suggesting the formation of an *hcp* phase within the nanoparticles, which is consistent with results from the XRD measurements (vide infra) [32].

In contrast, after photoirriadiation for 24 h by blue LEDs (455–475 nm), the size and shape of the silver nanoparticles exhibited a drastic change, as shown in Fig. 1b. First, one can see that the nanoparticles are now significantly larger and composed of a number of interesting shapes. For instance, both sharp-tipped and truncated triangular nanoprisms can be seen in the micrograph with the edge-lengths varying from 10 to 40 nm, as depicted in panel (D). Other unique nanostructures such as decahedra and tetrahedra can also be identified, which were likely formed by thickening and edge-selective fusion of the triangular nanoprisms [33, 34]. Such structures have also been observed in early studies and thought to originate from crystal twinning of the initial seed nanoparticles [25, 35–40]. For instance, Zheng et al. studied the effect of LED excitation wavelength on the shape distribution of the resulting nanostructures and found that under 455 nm photoirradiation, nanodecahedra were the predominant species, but when 519 nm light was used, triangular nanoprisms were the major species [38]. In the present study, the structural distribution (Figure S1) obtained from the TEM study presented above shows that decahedral nanoparticles accounted for only 27 % of all structures observed, whereas sharp-tipped and truncated triangular nanoprisms represented approximately 50 % of the population. In contrast, the overall yield of decahedral structures obtained by Zheng et al. was much higher (~ 90 %). This is likely due to their use of PVP as a shape-directing stabilizer, as it binds preferentially to silver {100} facets and likely promotes the growth of triangular nanoprisms into nanotetrahedra and their subsequent fusion into nanodecahedra.

Lattice fringes of the resulting silver nanostructures are also very well defined, as depicted by the high-resolution

TEM image in the inset to Fig. 1b, where *fcc* Ag(111) crystal planes can be identified with an interlayer spacing of 2.37 Å. Additionally, domains with a somewhat larger lattice spacing of 2.47 Å can also be seen (Figure S2). This might be attributed to internal stacking faults parallel to the basal {111} faces that created local *hcp* regions within the nanostructure and hence caused elongation along the {111} direction [41, 42]. Consistent results were obtained in XRD measurements (vide infra).

The structural evolution was manifested in UV–vis absorption spectroscopic measurements, as depicted in Fig. 2. It can be seen that for the seed nanoparticles (black curve), an absorption band at $\lambda_{max} = 390$ nm can be readily identified, which is the characteristic SPR of small silver nanoparticles [43]. Upon irradiation by the LED lights, the nanoparticle solution gradually changed in color from yellow to orange indicating the formation of anisotropic silver nanostructures. In fact, this might be monitored directly by acquiring the solution's UV–vis profiles over a 4 h irradiation period with a 30-min induction period as depicted in Fig. 2. One can see that upon photoirradiation, the absorption at 390 nm began to decline and concurrently, new peaks at 475 and 343 nm started to emerge and grow (black arrows), forming an isosbestic point at about 435 nm (red arrow). These new absorption features were characteristic of the in-plane dipole (475 nm), in-plane quadrupole (390 nm), and out-of-plane dipole (343 nm) plasmon resonances of silver nanoprisms, respectively [27, 29]. Similar absorption features have also been observed with silver nanotetrahedra and nanodecahedra [35, 38]. Additionally, the in-plane dipole resonance peak was found to blue shift somewhat over more prolonged irradiation time going from 475 nm after 4 h of irradiation to 465 nm after 24 h of irradiation, which is due to gradual truncation of the as-formed triangular nanoprisms. This truncation is caused by a decline of preferential in-plane growth, likely due to diminishing citrate concentration resulting in a decreasing surface coverage of the {111} facets by the protecting ligands, as well as gradual excitation of the in-plane quadruple SPR of existing triangular nanoprisms which caused localization of hot charge carriers along the edges of triangular nanoprisms and promoted growth perpendicular to the basal {111} planes of the structures [24, 44]. Note that once photoirradiation was turned off, the resulting faceted nanoparticles remained structurally stable in ambient as manifested by a virtually invariant UV–vis absorption profile.

More insights about the crystalline structures were obtained in XRD measurements. From Fig. 3, it can be seen that the faceted nanostructures (red curve) exhibited a series of diffraction peaks that are consistent with *fcc* silver (solid bars, JCPDS 00-004-0783) at 37.9° (111), 44.5° (200), 64.5° (220), and 77.5° (311). Three additional peaks can also be seen at 21.8°, 30.0°, and 34.4° that might be assigned to the diffractions of NaAgO (101), (310), and (311) crystalline planes (dotted bars, JCPDS 01-088-1567), respectively, suggesting the formation of silver oxide on the nanostructure surface. Furthermore, the faceted nanostructures also exhibited a broad peak at 39.2°, along with an even weaker one at 37.2° (labeled with asterisks), which suggests the formation of an *hcp* lattice arrangement, consistent with the TEM results presented above in Fig. 1 [32, 39, 42]. A similar diffraction profile can be seen with the seed nanoparticles as well (black curve), except that the diffraction for the silver oxide (330) at 40.9° became

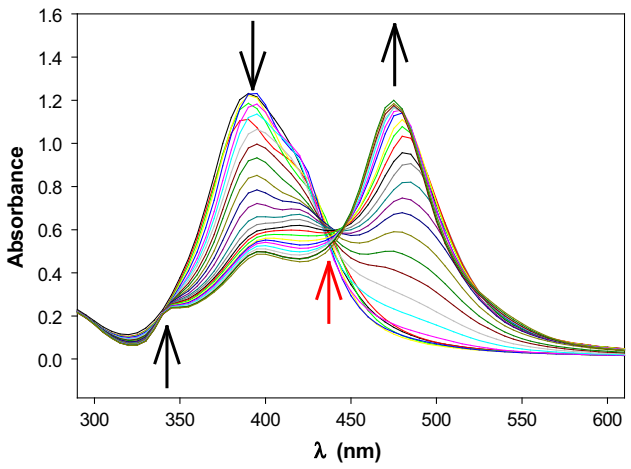

Fig. 2 UV–Vis spectra of a silver nanoparticle solution over a 4-h irradiation period illustrating the process of photo-conversion from spherical seed particles to nanoprisms. *Black arrows* signify the evolution of the absorption peaks and *red arrow* indicates the isosbestic point (Color figure online)

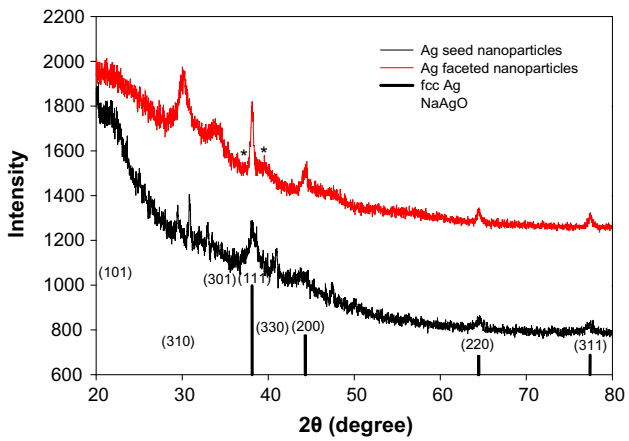

Fig. 3 XRD spectra of silver seed nanoparticles and faceted nanostructures with reference lines corresponding to *fcc* metallic silver and NaAgO obtained from the ICDD database. Asterisks signify the *hcp* peaks (Color figure online)

apparent, whereas the (301) peak at 34.4° diminished. One may also see that the Ag(111) diffraction peak was much more intense with the faceted nanostructures than with the seed nanoparticles, indicating a marked increase of the crystalline {111} facets, in agreement with HRTEM studies (Fig. 1) [45].

Overall, one can see an increase in size of the faceted nanostructures from the initial spherical particles after photoirradiation, as evidenced by measurements of the particle diameter if spherical and edge-length if triangular, tetragonal, or decahedral. This is expected as photoexcitation results in an increased rate of photo-induced redox cycles for structures having SPR modes in the LED emission range leading to growth along the planes of the excited SPR over time. This process is also reflected in the almost complete absence of spherical particles after 24 h of irradiation as oxidation of the small (<10 nm) particles provides the source of Ag^+ ions for nanoprism growth due to their lower redox potentials than those of larger particles [46, 47]. Due to this photo-mediated growth process, solutions irradiated for longer periods of time exhibited a higher concentration of silver nanostructures with surfaces composed primarily of {111} facets. These nanostructures therefore serve as an appropriate means by which to relate the nanoparticle surface structure to antimicrobial activity, as detailed below.

Antimicrobial activity

The antimicrobial activity of the silver seed nanoparticles and faceted nanostructures was then quantified and compared by monitoring the growth of *E. coli* cultures in liquid media over time. A 96-well plate with a dilution series of each sample was used to characterize the concentration dependence of relevant growth parameters. The most important of these parameters is the minimum inhibitory concentration (MIC), defined as the concentration of an antimicrobial agent at which bacterial cultures demonstrate no observed growth throughout the incubation period as evidenced by a lack of increase in optical density at 600 nm that corresponds to light scattering of bacterial cells. In this study, 20 μL of an *E. coli* suspension with an optical density of 0.1 at 600 nm (corresponding to an initial cell density of approximately 1.67×10^7 cells/mL [48]) in aqueous 20 mM HEPES was added to a dilution series of the silver seed nanoparticles and faceted nanostructures prepared by photoirradiation for 24 h. From the growth curves depicted in Fig. 4, two general trends were noted. First, from these growth curves, it is clear that solutions of both the as-prepared seed nanoparticles and LED-irradiated silver nanostructures exhibited an inhibitory effect on the growth of the *E. coli* colonies when compared with the blank control. Second, the faceted nanostructures clearly showed enhanced antimicrobial activity as compared to the seed nanoparticles, with an MIC of 4.9 and 5.4 mg/mL, respectively. This is somewhat surprising as the seed nanoparticles are much smaller in size than the faceted nanostructures (Fig. 1), and thus, with their greater effective surface area, one would anticipate greater membrane penetration capability. In fact, such a behavior has been observed by Agnihotri et al. in a study of the antimicrobial activity of silver nanoparticles within the size range of 5–100 nm [49]. However, in the present study, as depicted in Fig. 1c, d, size distributions acquired by analysis of TEM images show that the faceted nanostructures contained mostly particles between 20 and 40 nm in diameter/edge-length with only 10 % of the particles having a diameter less than 10 nm. In stark contrast, 80 % of the seed nanoparticles had a diameter of less than 5 nm and only 14 % having diameters greater than 10 nm. Therefore, the enhanced activity of the faceted nanostructures strongly suggests that surface morphologies might actually play a dominant role in the determination of the antimicrobial activity. As triangular nanoprisms, nanotetrahedra, and nanodecahedra are faceted predominantly by highly reactive {111} surfaces, these nanostructures exhibit an exceptionally strong affinity to sulfur-containing membrane proteins and oxygen-containing functional groups of lipopolysaccharide molecules which constitute 25 and 75 % of cell wall surfaces, respectively [21, 50, 51]. This would allow these highly faceted silver nanostructures to efficiently localize to *E. coli* cell walls, penetrate the outer membrane, and release silver ions into the periplasmic space. These ions would then bind to peptidoglycan polymers, resulting in disruption of cell wall synthesis and rapid entry of silver ions into the cytoplasm which allows silver to exert its toxic effects to intercellular targets such as DNA, as well as eventual membrane lysis from turgor pressure. Additionally, due to their large size, these nanostructures might easily cause a major disruption of the cell membrane once localized as they would interact with a greater number of cell wall targets per particle compared with the smaller, spherical seed nanoparticles. Localization of these larger structures to the cell walls would therefore result in physical membrane lysis through structural distortion as well as through free radical-induced peroxidation of membrane lipids, which has been suggested by previous studies [4, 52]. Furthermore, this membrane disruption might cause changes in membrane permeability which would adversely affect cellular respiration and inhibit the metabolism of bacterial cells, the effects of which could be observed in changes in the growth rate and the duration of lag phase for colonies treated with these silver nanostructures.

The growth of bacterial colonies is typically modeled as a first-order reaction:

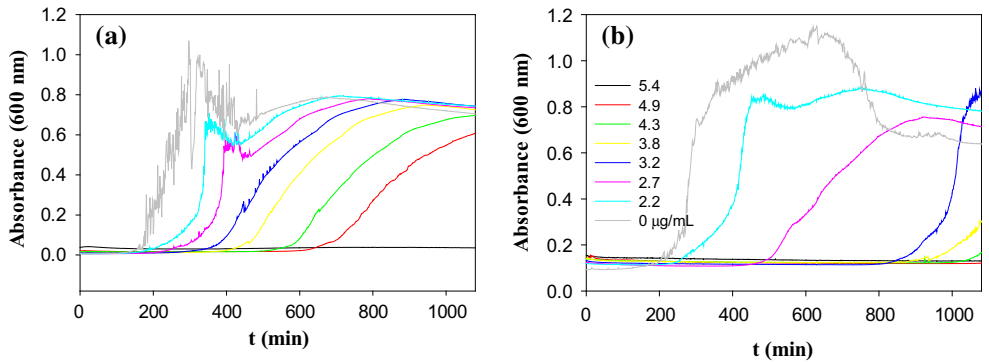

Fig. 4 Growth curves of *E. coli* cultures in Luria broth containing **a** silver seed nanoparticles and **b** faceted nanostructures formed by photoirradiation for 24 h. Nanoparticle concentrations are specified in figure legends (Color figure online)

$$\frac{dN}{dt} = kN, \tag{1}$$

where N is the number of bacteria at time t, and k is the first-order rate constant. As the optical density of bacteria is proportional to the concentration [48], this equation can be rearranged to

$$\ln\left(\frac{A}{Ao}\right) = kt, \tag{2}$$

where A and A_0 are the absorbance at 600 nm of the bacterial solution at time t and zero, respectively. Thus, a linear regression of $\ln(A/A_0)$ versus t should yield a quantitative assessment of the growth rate constant k of the bacterial culture. Additionally, the lag phase (t_L), defined as the time between inoculation and initiation of the log phase, is a measure of the amount of work required for a bacterial colony to adapt to its environment and provides another perspective by which to view changes in growth kinetics [53]. This value is typically measured from growth curves as the point at which the slope of the exponential growth phase intersects a horizontal line drawn from the initial absorbance value of the colony.

From the growth curves in Fig. 4, the values of growth rate constants were then calculated by linear regression, and the lag-phase durations were measured for *E. coli* in solutions of the as-prepared seed nanoparticles and faceted silver nanostructures. The results are shown graphically in Fig. 5 (and summarized in Table S1). A clear difference can be observed in the growth kinetics for *E. coli*, where faceted nanostructures (red bars) exhibited markedly enhanced activity in inhibiting bacterial growth than the as-prepared seed particles (black bars), with a lower growth rate constant (k) (i.e., slower growth) and longer lag-phase duration (t_L) at all particle concentrations, in good agreement with the MIC values estimated above. Notably, the difference in lag-phase duration is quite marked, with the silver seed nanoparticles having 2, 3, and 4 times shorter duration periods than the faceted nanostructures at 2.2, 2.7, and 3.2 µg/mL solution concentrations, respectively. At higher concentrations, this difference appears to decline going from less than three times the duration at 3.8 µg/mL to slightly above two times the duration at 4.3 µg/mL, indicating that a maximum growth inhibition occurred at lower concentrations. This is further supported by values of the growth rate constant calculated at these concentrations, with the most dramatic difference between the two silver nanostructure samples occurring at 2.7 µg/mL where the *E. coli* cultures treated with silver seed nanoparticles exhibited a growth rate constant of 6.0×10^{-3} min^{-1}, almost twice as much as that of the faceted nanostructures (3.1×10^{-3} min^{-1}).

Both solutions of silver nanostructures displayed a concentration at which they exerted their maximal effects on bacterial growth and lag-phase duration independently, with the growth rate being affected maximally at lower concentrations than lag-phase duration. This is expected as bacterial cells may withstand a certain degree of inhibition before having their growth drastically affected. Silver seed nanoparticles demonstrated their maximum decline in growth rate between 2.7 and 3.2 µg/mL at which growth rate constants decreased from 6.0×10^{-3} to 4.1×10^{-3} min^{-1} and a maximum increase in lag-phase duration between 3.8 and 4.3 µg/mL at which lag-phase duration increased by 145 min (from 305 to 450 min). The changes of these critical growth parameters occurred at lower concentration for the faceted nanostructure solutions, with a maximum decline in growth rate occurring between 2.2 and 2.7 µg/mL where growth rate constant decreased from 4.8×10^{-3} to 3.1×10^{-3} min^{-1} and a maximum increase in lag-phase duration between 2.7 and 3.2 µg/mL at which lag-phase duration increased by almost 6 h (from 450 to 805 min), respectively. This difference in critical concentrations at which these growth parameters are maximally affected is likely due to the different mechanisms of inhibition acting on the bacterial cells. Because silver seed nanoparticles are smaller and more prone to oxidation, they would affect bacterial cells primarily by releasing silver ions into and

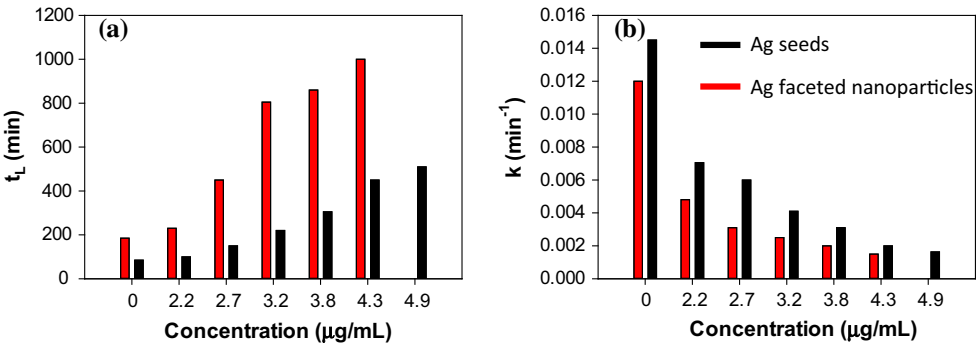

Fig. 5 **a** Lag-phase durations and **b** growth rate constants calculated from the growth curves in Fig. 4 for the seed nanoparticles (*black bars*) and the photoirradiated nanostructures (*red bars*) at various concentrations (Color figure online)

around the bacterial cells which will subsequently penetrate the outer-membrane and bind respiratory chain dehydrogenases embedded in the inner-membrane [8, 54]. This mechanism is supported by surface-enhanced Raman spectroscopy (SERS) studies performed by Zeiri et al. which suggest that silver ions localize near flavin-containing cellular components, two of which are likely NADH:ubiquinone oxidoreductase and succinate dehydrogenase that contain flavin mononucleotide and flavin adenine dinucleotide, respectively [55]. This is particularly likely as both of these proteins contain a high density of sulfur-containing moieties such as structurally significant cysteine residues and a large number of iron-sulfur clusters involved in their redox processes [56, 57]. Binding of silver ions to these proteins likely causes a severe disruption of their function and eventually leads to a complete collapse of membrane-potential through leakage of protons and intracellular potassium ions [58–60]. In contrast, faceted silver nanostructures are much larger and, due to their highly {111} faceted surface structure, have an enhanced affinity for the oxygen-containing groups of the O-antigen domain of lipopolysaccharide molecules resulting in attractive forces which allow for rapid localization to gram-negative bacterial outer membranes. This is advantageous as these nanostructures will more likely have a significant portion of their mass intact upon localizing to a bacterial cell resulting in a much larger silver ion reservoir at the site of activity. Upon localization, these structures could also exert additional structural damage by binding to OmpA and Lpp proteins which are major constituents of the outer-membrane and provide a physical linkage between the outer-membrane and the peptidoglycan layer [58, 61]. Because these proteins cover much of the surface, large silver nanostructures can bind to multiple units and cause severe perturbation of the outer-membrane structure resulting in pit formation and cell lysis [54]. Because these larger nanostructures can physically lyse bacterial cells as well, a lower concentration is required to cause severe inhibitory effects and is reflected in both the larger change in lag-phase duration, and lower MIC values. Both seed and faceted nanostructures have similar maximal decreases in growth rate constant, and this could be attributed to the role of the inhibitory actions of silver ions that dominate at lower concentrations as the probability of large silver nanostructures localizing to a significant population of bacterial cells is low. This supports the idea of faceted silver nanostructures having an enhanced inhibitory effect on bacterial growth via additional membrane disruption mechanisms, despite a marked increase in size, and warrants a closer investigation in future studies as to the exact processes responsible for this activity. Comprehensive elucidation of these underlying mechanisms will require additional transcriptomics and thorough microscopic studies of silver nanostructure-treated bacterial cells.

Conclusion

A variety of faceted silver nanostructures, including triangular nanoprisms, nanodecahedra, and nanobipyramids were synthesized by photoirradiation of silver seed nanoparticles with blue LEDs and demonstrated enhanced antimicrobial activity when compared with smaller, spherical silver nanoparticles. TEM studies revealed that these nanostructures had predominantly {111} faceted surfaces which not only aided in binding to bacterial cell walls but also in the dissolution of silver ions into bacterial cells. Growth kinetics measurements revealed that the faceted silver nanostructures demonstrated a lower MIC as well as lower concentrations at which growth rate constant and lag-phase duration were critically affected. This is postulated to be due to larger, {111} faceted silver nanostructures that caused physical disruption of bacterial cell walls through binding of outer-membrane proteins crucial for cell wall integrity in addition to the typical inhibitory mechanisms exhibited by ionic silver. These findings suggest that the antimicrobial activity of silver nanostructures is more structure-dependent than is generally accepted and provides a biochemical basis for this. Further inquiry into the effects of {111} faceted silver nanostructures on the cellular components of bacterial cells will shed light on these mechanisms.

Acknowledgements This work was supported in part by the National Science Foundation (CHE-1012258, CHE-1265635 and DMR-1409396). TEM work was carried out at the National Center for Electron Microscopy at the Lawrence Berkeley National Laboratory as part of a user project. The PXRD data in this work were recorded on a Rigaku SmartLab instrument supported by the NSF Major Research Instrumentation (MRI) Program under Grant DMR-1126845.

References

1. Alexander JW (2009) History of the medical use of silver. Surg Infect (Larchmt) 10(3):289–292. doi:10.1089/sur.2008.9941
2. Russell AD, Hugo WB (1994) Antimicrobial activity and action of silver. Prog Med Chem 31:351–370
3. Maillard JY, Hartemann P (2013) Silver as an antimicrobial: facts and gaps in knowledge. Crit Rev Microbiol 39(4):373–383. doi:10.3109/1040841X.2012.713323
4. Marambio-Jones C, Hoek EMV (2010) A review of the antibacterial effects of silver nanomaterials and potential implications for human health and the environment. J Nanopart Res 12(5):1531–1551. doi:10.1007/s11051-010-9900-y
5. Kim JS, Kuk E, Yu KN, Kim JH, Park SJ, Lee HJ, Kim SH, Park YK, Park YH, Hwang CY, Kim YK, Lee YS, Jeong DH, Cho MH (2007) Antimicrobial effects of silver nanoparticles. Nanomedicine 3(1):95–101. doi:10.1016/j.nano.2006.12.001
6. Xu FF, Imlay JA (2012) Silver(I), mercury(II), cadmium(II), and zinc(II) target exposed enzymic iron-sulfur clusters when they toxify *Escherichia coli*. Appl Environ Microbiol 78(10): 3614–3621. doi:10.1128/AEM.07368-11
7. Liau SY, Read DC, Pugh WJ, Furr JR, Russell AD (1997) Interaction of silver nitrate with readily identifiable groups: relationship to the antibacterial action of silver ions. Lett Appl Microbiol 25(4):279–283
8. Holt KB, Bard AJ (2005) Interaction of silver(I) ions with the respiratory chain of *Escherichia coli*: an electrochemical and scanning electrochemical microscopy study of the antimicrobial mechanism of micromolar Ag^{+}. Biochemistry 44(39):13214–13223. doi:10.1021/bi0508542
9. Petering HG (1976) Pharmacology and toxicology of heavy-metals—Silver. Pharmacol Ther Pt A 1(2):127–130. doi:10.1016/0362-5478(76)90002-4
10. Schreurs WJ, Rosenberg H (1982) Effect of silver ions on transport and retention of phosphate by *Escherichia coli*. J Bacteriol 152(1):7–13
11. Yamane T, Davidson N (1962) On the complexing of deoxyribonucleic acid by silver (I). Biochim Biophys Acta 55:609–621
12. Kvitek L, Panacek A, Soukupova J, Kolar M, Vecerova R, Prucek R, Holecova M, Zboril R (2008) Effect of surfactants and polymers on stability and antibacterial activity of silver nanoparticles (NPs). J Phys Chem C 112(15):5825–5834. doi:10.1021/Jp711616v
13. Raffi M, Hussain F, Bhatti TM, Akhter JI, Hameed A, Hasan MM (2008) Antibacterial characterization of silver nanoparticles against *E. coli* ATCC-15224. J Mater Sci Technol 24(2):192–196
14. Smetana AB, Klabunde KJ, Marchin GR, Sorensen CM (2008) Biocidal activity of nanocrystalline silver powders and particles. Langmuir 24(14):7457–7464. doi:10.1021/la800091y
15. Vertelov GK, Krutyakov YA, Efremenkova OV, Olenin AY, Lisichkin GV (2008) A versatile synthesis of highly bactericidal Myramistin(R) stabilized silver nanoparticles. Nanotechnology 19(35):355707. doi:10.1088/0957-4484/19/35/355707
16. Porel S, Ramakrishna D, Hariprasad E, Gupta AD, Radhakrishnan TP (2011) Polymer thin film with in situ synthesized silver nanoparticles as a potent reusable bactericide. Curr Sci India 101(7):927–934
17. Jones SA, Bowler PG, Walker M, Parsons D (2004) Controlling wound bioburden with a novel silver-containing Hydrofiber dressing. Wound Repair Regen 12(3):288–294. doi:10.1111/j.1067-1927.2004.012304.x
18. Leaper DJ (2006) Silver dressings: their role in wound management. Int Wound J 3(4):282–294. doi:10.1111/j.1742-481X.2006.00265.x
19. Morones JR, Elechiguerra JL, Camacho A, Holt K, Kouri JB, Ramirez JT, Yacaman MJ (2005) The bactericidal effect of silver nanoparticles. Nanotechnology 16(10):2346–2353. doi:10.1088/0957-4484/16/10/059
20. Pal S, Tak YK, Song JM (2007) Does the antibacterial activity of silver nanoparticles depend on the shape of the nanoparticle? A study of the Gram-negative bacterium *Escherichia coli*. Appl Environ Microbiol 73(6):1712–1720. doi:10.1128/AEM.02218-06
21. Horswell SL, Pinheiro AL, Savinova ER, Danckwerts M, Pettinger B, Zei MS, Ertl G (2004) A comparative study of hydroxide adsorption on the (111), (110), and (100) faces of silver with cyclic voltammetry, ex situ electron diffraction, and in situ second harmonic generation. Langmuir 20(25):10970–10981. doi:10.1021/la0483818
22. Jin R, Cao Y, Mirkin CA, Kelly KL, Schatz GC, Zheng JG (2001) Photoinduced conversion of silver nanospheres to nanoprisms. Science 294(5548):1901–1903. doi:10.1126/science.1066541
23. Thrall ES, Steinberg AP, Wu XM, Brus LE (2013) The role of photon energy and semiconductor substrate in the plasmon-mediated photooxidation of citrate by silver nanoparticles. J Phys Chem C 117(49):26238–26247. doi:10.1021/Jp409586z
24. Xue C, Metraux GS, Millstone JE, Mirkin CA (2008) Mechanistic study of photomediated triangular silver nanoprism growth. J Am Chem Soc 130(26):8337–8344. doi:10.1021/ja8005258
25. Lu HF, Zhang HX, Yu X, Zeng SW, Yong KT, Ho HP (2012) Seed-mediated Plasmon-driven Regrowth of Silver Nanodecahedrons (NDs). Plasmonics 7(1):167–173. doi:10.1007/s11468-011-9290-8
26. Pastoriza-Santos I, Liz-Marzan LM (2008) Colloidal silver nanoplates. State of the art and future challenges. J Mater Chem 18(15):1724–1737. doi:10.1039/B716538b
27. Jin R, Cao YC, Hao E, Metraux GS, Schatz GC, Mirkin CA (2003) Controlling anisotropic nanoparticle growth through plasmon excitation. Nature 425(6957):487–490. doi:10.1038/nature02020
28. Millstone JE, Hurst SJ, Metraux GS, Cutler JI, Mirkin CA (2009) Colloidal gold and silver triangular nanoprisms. Small 5(6):646–664. doi:10.1002/smll.200801480
29. Callegari A, Tonti D, Chergui M (2003) Photochemically grown silver nanoparticles with wavelength-controlled size and shape. Nano Lett 3(11):1565–1568. doi:10.1021/nl034757a
30. Bastys V, Pastoriza-Santos I, Rodriguez-Gonzalez B, Vaisnoras R, Liz-Marzan LM (2006) Formation of silver nanoprisms with surface plasmons at communication wavelengths. Adv Funct Mater 16(6):766–773
31. Khan MAM, Kumar S, Ahamed M, Alrokayan SA, AlSalhi MS (2011) Structural and thermal studies of silver nanoparticles and electrical transport study of their thin films. Nanoscale Res Lett 6. Artn 434. doi:10.1186/1556-276x-6-434
32. Liu T, Li DS, Yang DR, Jiang MH (2011) Preparation of echinus-like SiO_2@Ag structures with the aid of the HCP phase. Chem Commun 47(18):5169–5171. doi:10.1039/C1cc10401b
33. McEachran M, Kitaev V (2008) Direct structural transformation of silver platelets into right bipyramids and twinned cube nanoparticles: morphology governed by defects. Chem Commun (Camb) 44:5737–5739. doi:10.1039/b813519c
34. Gao Y, Jiang P, Song L, Wang JX, Liu LF, Liu DF, Xiang YJ, Zhang ZX, Zhao XW, Dou XY, Luo SD, Zhou WY, Xie SS

(2006) Studies on silver nanodecahedrons synthesized by PVP-assisted *N*, *N*-dimethylformamide (DMF) reduction. J Crystal Growth 289(1):376–380. doi:10.1016/j.jcrysgro.2005.11.123
35. Zhang J, Li S, Wu J, Schatz GC, Mirkin CA (2009) Plasmon-mediated synthesis of silver triangular bipyramids. Angew Chem Int Ed Engl 48(42):7787–7791. doi:10.1002/anie.200903380
36. Wiley BJ, Xiong Y, Li ZY, Yin Y, Xia Y (2006) Right bipyramids of silver: a new shape derived from single twinned seeds. Nano Lett 6(4):765–768. doi:10.1021/nl060069q
37. Pietrobon B, Kitaev V (2008) Photochemical synthesis of monodisperse size-controlled silver decahedral nanoparticles and their remarkable optical properties. Chem Mater 20(16): 5186–5190. doi:10.1021/Cm800926u
38. Zheng X, Zhao X, Guo D, Tang B, Xu S, Zhao B, Xu W, Lombardi JR (2009) Photochemical formation of silver nanodecahedra: structural selection by the excitation wavelength. Langmuir 25(6):3802–3807. doi:10.1021/la803814j
39. Rocha TCR, Zanchet D (2007) Structural defects and their role in the growth of Ag triangular nanoplates. J Phys Chem C 111(19):6989–6993. doi:10.1021/Jp0702696
40. Zhou J, An J, Tang B, Xu S, Cao Y, Zhao B, Xu W, Chang J, Lombardi JR (2008) Growth of tetrahedral silver nanocrystals in aqueous solution and their SERS enhancement. Langmuir 24(18):10407–10413. doi:10.1021/la800961j
41. Germain V, Li J, Ingert D, Wang ZL, Pileni MP (2003) Stacking faults in formation of silver nanodisks. J Phys Chem B 107(34):8717–8720
42. Aherne D, Ledwith DM, Gara M, Kelly JM (2008) Optical properties and growth aspects of silver nanoprisms produced by a highly reproducible and rapid synthesis at room temperature. Adv Funct Mater 18(14):2005–2016. doi:10.1002/adfm.200800233
43. Creighton JA, Eadon DG (1991) Ultraviolet visible absorption-spectra of the colloidal metallic elements. J Chem Soc Faraday Trans 87(24):3881–3891
44. Kelly KL, Coronado E, Zhao LL, Schatz GC (2003) The optical properties of metal nanoparticles: the influence of size, shape, and dielectric environment. J Phys Chem B 107(3):668–677. doi:10.1021/Jp026731y
45. Xu S, Tang B, Zheng X, Zhou J, An J, Ning X, Xu W (2009) The facet selectivity of inorganic ions on silver nanocrystals in etching reactions. Nanotechnology 20(41):415601. doi:10.1088/0957-4484/20/41/415601
46. Gutierrez M, Henglein A (1993) Formation of colloidal silver by push-pull reduction of Ag^{+}. J Phys Chem 97(44):11368–11370. doi:10.1021/J100146a003
47. Jiang ZJ, Liu CY, Li YJ (2004) Electrochemical studies of silver nanoparticles tethered on silica sphere. Chem Lett 33(5):498–499
48. Sezonov G, Joseleau-Petit D, D'Ari R (2007) *Escherichia coli* physiology in Luria–Bertani broth. J Bacteriol 189(23):8746–8749. doi:10.1128/Jb.01368-07
49. Agnihotri S, Mukherji S, Mukherji S (2014) Size-controlled silver nanoparticles synthesized over the range 5–100 nm using the same protocol and their antibacterial efficacy. RSC Adv 4(8):3974–3983. doi:10.1039/C3ra44507k
50. Feng QL, Wu J, Chen GQ, Cui FZ, Kim TN, Kim JO (2000) A mechanistic study of the antibacterial effect of silver ions on *Escherichia coli* and *Staphylococcus aureus*. J Biomed Mater Res 52(4):662–668. doi:10.1002/1097-4636(20001215)52:4<662:AID-JBM10>3.0.CO;2-3
51. Rietschel ET, Kirikae T, Schade FU, Mamat U, Schmidt G, Loppnow H, Ulmer AJ, Zahringer U, Seydel U, Di Padova F et al (1994) Bacterial endotoxin: molecular relationships of structure to activity and function. FASEB J 8(2):217–225
52. Park HJ, Kim JY, Kim J, Lee JH, Hahn JS, Gu MB, Yoon J (2009) Silver-ion-mediated reactive oxygen species generation affecting bactericidal activity. Water Res 43(4):1027–1032. doi:10.1016/j.watres.2008.12.002
53. Robinson TP, Ocio MJ, Kaloti A, Mackey BM (1998) The effect of the growth environment on the lag phase of Listeria monocytogenes. Int J Food Microbiol 44(1–2):83–92 S0168-1605(98)00120-2
54. Li WR, Xie XB, Shi QS, Zeng HY, Ou-Yang YS, Chen YB (2010) Antibacterial activity and mechanism of silver nanoparticles on *Escherichia coli*. Appl Microbiol Biotechnol 85(4): 1115–1122. doi:10.1007/s00253-009-2159-5
55. Zeiri L, Bronk BV, Shabtai Y, Eichler J, Efrima S (2004) Surface-enhanced Raman spectroscopy as a tool for probing specific biochemical components in bacteria. Appl Spectrosc 58(1):33–40. doi:10.1366/000370204322729441
56. Friedrich T (1998) The NADH:ubiquinone oxidoreductase (complex I) from *Escherichia coli*. Biochim Biophys Acta 1364(2):134–146
57. Cecchini G, Schroder I, Gunsalus RP, Maklashina E (2002) Succinate dehydrogenase and fumarate reductase from *Escherichia coli*. Biochim Biophys Acta 1553(1–2):140–157
58. Koebnik R, Locher KP, Van Gelder P (2000) Structure and function of bacterial outer membrane proteins: barrels in a nutshell. Mol Microbiol 37(2):239–253
59. Lok CN, Ho CM, Chen R, He QY, Yu WY, Sun H, Tam PK, Chiu JF, Che CM (2006) Proteomic analysis of the mode of antibacterial action of silver nanoparticles. J Proteome Res 5(4): 916–924. doi:10.1021/pr0504079
60. Letellier L, Shechter E (1979) Cyanine dye as monitor of membrane potentials in *Escherichia coli* cells and membrane vesicles. Eur J Biochem 102(2):441–447
61. Sonntag I, Schwarz H, Hirota Y, Henning U (1978) Cell envelope and shape of *Escherichia coli*: multiple mutants missing the outer membrane lipoprotein and other major outer membrane proteins. J Bacteriol 136(1):280–285